An experimental and theoretical investigation of the influence of surface roughness on corrosion in CO₂ environments

Mohammed Al-Khateeb*, Richard Barker, Anne Neville, Harvey Thompson
Institute of Functional Surfaces, School of Mechanical Engineering, University of Leeds, Leeds, LS2 9JT

mnmaak@leeds.ac.uk

1.   Abstract

The influence of surface roughness on the rate of corrosion in CO_2 environments in the absence of protective film formation is investigated both experimentally and theoretically. The former measurements are obtained using the Linear Polarisation Resistance technique on a Rotating Cylinder Electrode apparatus with four different samples with roughness of 0.5, 6, 20 and 35μm. Experimental measurements of corrosion rate for smooth and rough surfaces are compared against predictions from a modified form of a CO_2 corrosion model [1], where mass transfer coefficients are specified using a new correlation for rough surfaces [2], which accounts for both the influence of the total surface area and enhancement of the mass-transfer process. Test conditions selected for comparison consisted of a CO_2-saturated 1 wt.% NaCl brine at 25ºC covering pH values between 4 and 6. X65 carbon steel samples were used as working electrodes, with rotational rates varying from 1000 to 4000 rpm. Agreement between experimental and theoretical corrosion rates is very good and demonstrates clearly how increased surface roughness accentuates corrosion rates and the need for considering surface topography when making reliable corrosion predictions when implementing theoretical models.

Keywords: Electro-chemical modelling, experiments, surface roughness.

2.   Introduction

CO₂ corrosion of steel in oil and gas production and transportation systems is an important issue of practical and commercial interest. When CO₂ dissolves in brines it permits the formation of carbonic acid which is corrosive towards equipment

made from carbon steel. This process is capable of affecting asset integrity, the environment and safety of personnel [3].

In the context of oil and gas pipelines, the surface roughness of steel pipelines delivered to coating yards can be in the order of $20\mu m$ and may even exceed $50\mu m$ [4], yet laboratory experiments in CO_2 environments tend to be with samples which are wet-ground to sub-micron surface finishes (i.e. 1200 grit SiC paper). This is despite the fact that the effect of surface roughness is believed to contribute significantly towards corrosion rates in CO_2-containing environments [5] based on the notion that surface topography can affect the hydrodynamic and mass-transfer boundary layer which can influence the electrochemical response of the corroding material.

A review of the literature reveals that surface roughness is actually believed to control the rate of mass transfer to surfaces, as opposed to the geometry of the system itself. These effects have been quantified using several empirical correlations linking the Sherwood, Reynolds and Schmidt numbers, see e.g. Poulson [6]. An assessment of the influence of roughness on mass-transfer characteristics has been conducted on geometries such as rectangular ducts [7], pipes [8], the rotating disk [9] and the rotating cylinder electrode (RCE) [10], the latter of which is the focus of this study. The general consensus of these studies is that rougher surfaces lead to an accentuation in mass-transfer and hence, the rate of material dissolution in diffusion-controlled processes.

Research as early as the 1930s by King and Howard [11] demonstrated that in diffusion-controlled environments, surface roughness has a major effect on enhancing the rate of metal dissolution. These observations are also supported by the work of Ibl [12] and by Brenan and Trass [13] in the 1960s who studied the effect of roughness on the dissolution of crystalline surfaces with different degrees of roughness. Their results showed that the rate of mass transfer increased fourfold with the increase in surface roughness height from ~2.5 to 10 µm over a Reynolds number range from 8,000 to 60,000.

Regardless of initial internal surface conditions of the pipeline, multiphase flow environments have also been shown to increase pipe wall internal surface roughness, resulting in an increase in mass transfer [6]. Such behaviour was also observed by Postlethwaite and Lotz [8] in erosion-corrosion experiments in aerated

2

aqueous slurries of sand. Both authors concluded that the mass transfer would be affected by the surface roughness produced by erosion-corrosion in the presence of sand particles, accentuating corrosion of carbon steel.

Given that some of the electrochemical processes on carbon steel surfaces in CO_2 environments are influenced by mass-transfer (particularly in solutions close to pH 4), and that numerous studies have shown rough surfaces can enhance mass-transfer, there is clearly a need for greater awareness and fundamental understanding of the role of surface roughening on corrosion rates in CO_2 environments and how this relates to the transport of species to and from the steel surface and the impact that this has on material dissolution.

In relation to experimentally observing the effect of surface roughness, the RCE provides a convenient means of generating a uniform reaction environment for fundamental and engineering studies of corrosion and mass-transfer under open-circuit, controlled potential or constant current conditions, and is the experimental apparatus of choice for this study. The recent review by Walsh et al. [14] provides a comprehensive summary of the range of applications and previous experimental studies in RCE geometries.

This present paper utilises the Linear Polarisation Resistance (LPR) technique in conjunction with the RCE to study the effect of surface roughness on carbon steel corrosion rate in CO_2 environments. It extends the recent experimental study of Al-Khateeb et al [2], who explored the influence of surface roughness and total surface area on mass-transfer through the application of the limiting current technique for a range of rotational speeds in NaCl solutions saturated either with N_2 or CO_2 at pH=3 and pH=4. The previous paper by Al-Khateeb [2] provides reliable benchmark mass-transfer data, which is used in this work to assist in the construction of a theoretical CO_2 corrosion prediction model for rough surfaces which are then assessed and validated against electrochemical corrosion measurements. This data will be useful since properly-validated corrosion models can be useful for improving the design of pipeline networks and infrastructure for oil and gas production and processing. This is a key consideration informing major design decisions, such as material selection and pipeline thickness, as well as the need for corrosion mitigation equipment and strategies.

The recent review of CO_2 corrosion models by Kahyarian et al. [15] identified three categories: *empirical*, *semi-empirical* and *mechanistic*. Empirical/semi-empirical ones are simple models, developed when there is limited fundamental understanding of the physical phenomena, often taking the form of statistical fits based on experimental data or correlation factors. Although these can be useful for representative conditions for which they have been designed, they should be used with caution outside their range of application. Important examples of empirical/semi-empirical models include those of deWaard & Milliams [16] and Pots et al. [17] A number of useful reviews of such models have appeared in the literature, see e.g. Olson [18] and Nesic [19].

A number of mechanistic models have been developed to provide a physical basis for corrosion rate predictions and to address the inherent limitations of empirical and semi-empirical models [15]. Elementary mechanistic models de-couple the main physicochemical phenomena in corrosion processes, namely mass-transfer, charge-transfer and chemical reactions, and use parameters which have a sound theoretical foundation. Examples of these are widely used in corrosion engineering analyses (see e.g. Sundaram et al. [20], Han et al. [21]) but their neglect of homogeneous chemical reactions is a serious shortcoming.

These limitations have been addressed in more comprehensive mechanistic models based on the Nernst-Planck equation for mass conservation. Nordsveen et al. [5] solved the Nernst-Planck equation to describe the time-dependent mass-transfer of species in the boundary layer using a computationally expensive multi-node approach. The computational requirements of their multi-node approach were alleviated by Remita et al. [22] who used a simplified, steady-state form of the Nordsveen et al. [5] model, which may be sufficient for practical purposes of corrosion rate estimation. Zheng et al. [1] recently proposed a novel, and much more computationally efficient 2-node approach to predicting corrosion rates in cases of mixed CO_2/H_2S corrosion, which calculates the surface concentrations and corrosion rates at corroding surfaces using mass-transfer coefficients and bulk concentrations of each species. This paper uses a new correlation based on the 2-node approach for mass-transfer coefficients in RCE environments with rough surfaces to predict corrosion rates for comparison with the experimental data gathered.

The paper is organised as follows. The experimental methods and RCE experiments are first described before the corrosion modelling strategy is described and validated. A series of experimental and computational results are then presented which explore the effect of surface roughness, RCE velocity and pH on corrosion rate at a temperature of 25°C in a CO_2-saturated 1 wt.% NaCl brine. Finally, conclusions are drawn.

3.   Experimental Methods

Four RCE samples with different surface finishes were prepared by machining each sample on a lathe and applying discrete and carefully controlled pressures on the tool holder. The electrodes were carbon steel X65 with 1.2 cm diameter and 1 cm length. The surface texture of the samples was analysed using white light interferometry, a non-contact optical technique for surface height measurements which is capable or resolving surface topography down to nanometer accuracy. The specification of the samples are given in Table 1, with images of the samples and an example of the profilometry data provided in Figure 1. Where (e) is average distance from peak to valley and (A_R/A_P) is ratio of true surface area of rough electrode projected surface area of electrode.

Table 1 RCE surface properties of the four samples considered in this study.

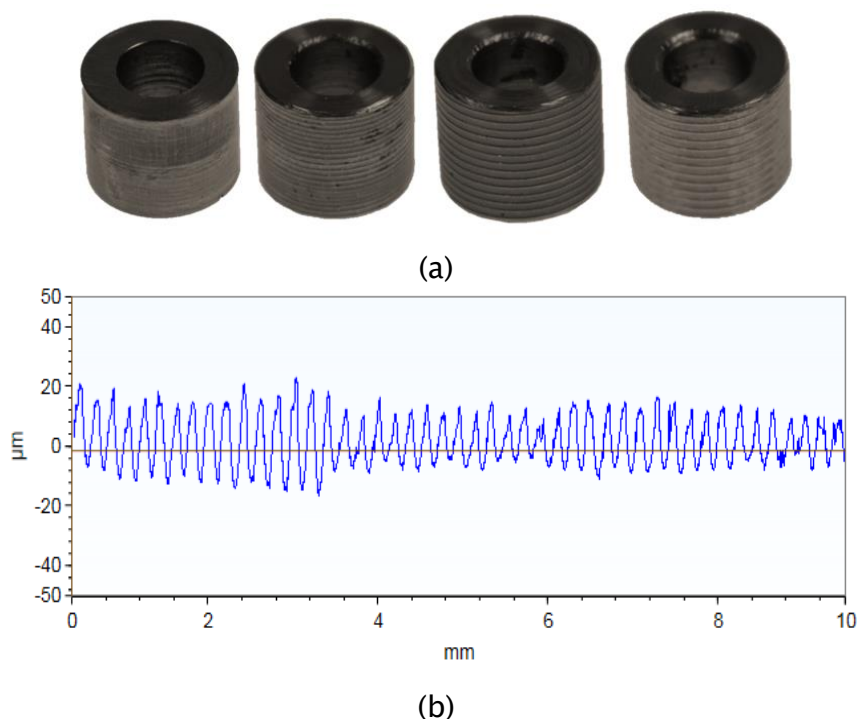| Sample	Roughness height (e) μm	(d/e)	(A_R/A_P)
Smooth	0.5	24000	1.004
Rough	6	2000	1.108
	20	600	1.219
	34	353	1.234

(a)

(b)

Figure 1 (a) Images of the RCE samples with different surfaces roughnesses of 0.5, 6, 20 and 35 μm and (b) example 2D output from profilometry analysis of 6 μm roughness sample

Experiments were conducted in a 1L glass cell at atmospheric pressure and 25°C. The three electrode setup shown in Figure 2 was employed for all experiments, which comprises a working electrode (RCE sample), a reference electrode (Ag/AgCl) and a counter electrode (platinum). Electrochemical measurements were performed using an ivium compactstat connected with a computer.

The tests were performed at rotational velocities between 1000 and 4000 rpm in a 1 wt.% NaCl solution saturated with carbon dioxide (CO_2) gas for 24 hours prior to the experiments to ensure that the system was sufficiently free from oxygen. Bubbling of gas into the electrolyte was also maintained over the duration of each experiment and temperature was controlled with the aid of a hotplate and thermocouple. The pH of the system was initially measured using a pH probe directly immersed into the electrolyte and adjusted to the desired value using sodium bicarbonate ($NaHCO_3$). The full matrix of test conditions evaluated is provided in Table 2.

Table 2 Experimental test matrix.

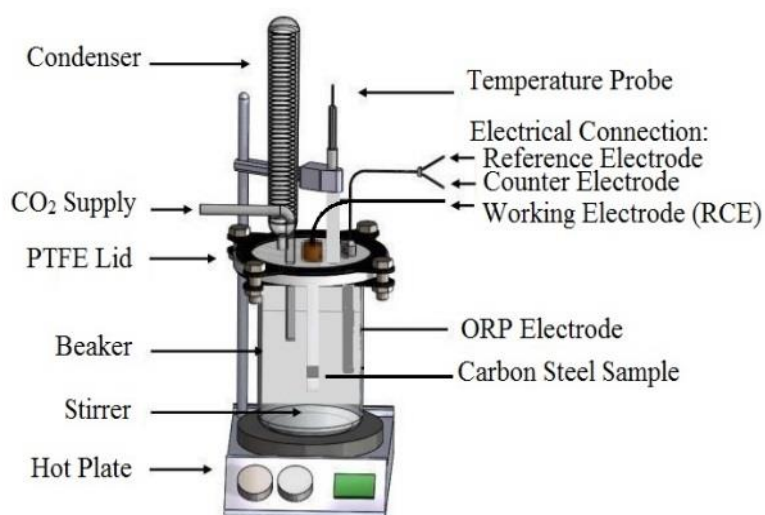| Working Environment	CO_2
pH	4–6
Temperature	25°C
Total Pressure	1 bar
NaCl Concentration	1 wt.%
Rotation Speed	1000 – 4000 rpm

Figure 2 Schematic of RCE three electrode cell.

Prior to each experiment the samples were degreased with acetone, rinsed with distilled water and then dried with compressed air before mounting onto the RCE shaft. The open circuit potential of the material was then allowed to stabilise for 10

minutes before starting each experiment. Following stabilisation of the OCP, *in situ* corrosion rates were recorded by means of the DC LPR technique. LPR measurements were conducted by polarising the sample ±15 mV vs. the open circuit potential, scanning at a rate of 0.25 mV/s to obtain a polarisation resistance, R_p (Ohm.cm^2). LPR measurements were undertaken every 10 minutes over a total period of 3 h.

In all experiments, the solution resistance, R_s (Ohm.cm^2) was determined after LPR measurements were complete using electrochemical impedance spectroscopy (EIS). This consisted of polarising the sample ±5 mV vs. the OCP using a frequency range from 20 kHz to 0.1 Hz. The value of R_s was subtracted from R_p to produce a charge-transfer resistance, R_{ct} (Ohm.cm^2) which was used to determine the corrosion rate behaviour with time:

$$R_{ct} = R_p - R_s \qquad (1)$$

Potentiodynamic measurements were also performed on each sample at the end of the 3 h test. This technique was used to generate Tafel polarisation curves to determine the anodic and cathodic Tafel constants (β_a and β_c, respectively in mV/decade) and ultimately an appropriate Stern-Geary coefficient (B) to enable calculation of corrosion rates from the values of R_{ct} determined as a function of time in each experiment.

Tafel polarisation curves were also collected by performing individual anodic and cathodic sweeps starting at OCP and scanning to either 250 mV or –500 mV vs. OCP, respectively at a scan rate of 0.5 mV/s. Only one Tafel curve (either anodic or cathodic) was generated at the end of each experiment as significant polarisation can alter the surface characteristics and/or result in contamination of the test solution.

From the polarisation curves produced, it was possible to determine β_a and β_c by measuring their respective gradients over regions were linearity was observed between the applied voltage and the natural log of the measured current. The Tafel slope measurements were used to determine the Stern-Geary coefficient (B), and the corrosion current density, i_{corr} (mA/cm^2):

$$B = \frac{\beta_a \beta_c}{2.303(\beta_a + \beta_c)} \qquad (2)$$

$$i_{corr} = \frac{\beta_a \beta_c}{2.303 R_{ct}(\beta_a + \beta_c)} \qquad (3)$$

where β_a and β_c are the coefficients which characterize the anodic and cathodic Tafel slopes of corrosion process in (V). The i_{corr} value obtained was used in combination with Faraday's Law and the measured values of R_{ct} to determine the corrosion rate (CR) in mm/year

$$CR = \frac{3.27 i_{corr} M_{Fe}}{n\rho} \qquad (4)$$

Where 3.27 is a conversion factor (mm.g/(mA.cm.year)), M_{Fe} is the atomic mass of iron = 55.845 g/mol, n=2 is the number of electrons generated in the anodic reaction and ρ the density of iron (g/cm³).

Each experiment was repeated at least twice and the values of corrosion rate reported in this work reflect the average of multiple LPR measurements over both 3 hour tests complete with errors bars which indicate the maximum and minimum corrosion rates determined from the individual measurements across all experiments.

4.   Corrosion Modelling

The experimental measurements of the effect of surface roughness on corrosion rate are compared with predictions based on the computationally-efficient 2-node approach, proposed recently by Zheng et al. [1], which calculates species concentrations at the corroding surface in a thin surface water film of thickness Δx by accounting for homogeneous chemical reactions, mass-transfer of species and electro-chemical reactions at the corroding surface. This leads to the equation

$$\frac{\partial c_{s,j}}{\partial t} = \frac{(N_{in,j} - N_{out,j})}{\Delta x} + R_j \qquad (5)$$

where $c_{s,j}$ is the surface concentration of species j, $N_{in,j}$ is the flux of species j from the bulk into the surface water film, $N_{out,j}$ is the flux of species out of the surface water film due to the electro-chemical reactions and R_j is the rate of chemical reaction of species j in the surface water film, see Figure 3. There are 7 species to be accounted for, namely CO_2, H_2CO_3, HCO_3^-, CO_3^{2-}, OH^-, H^+ and Fe^{2+}.
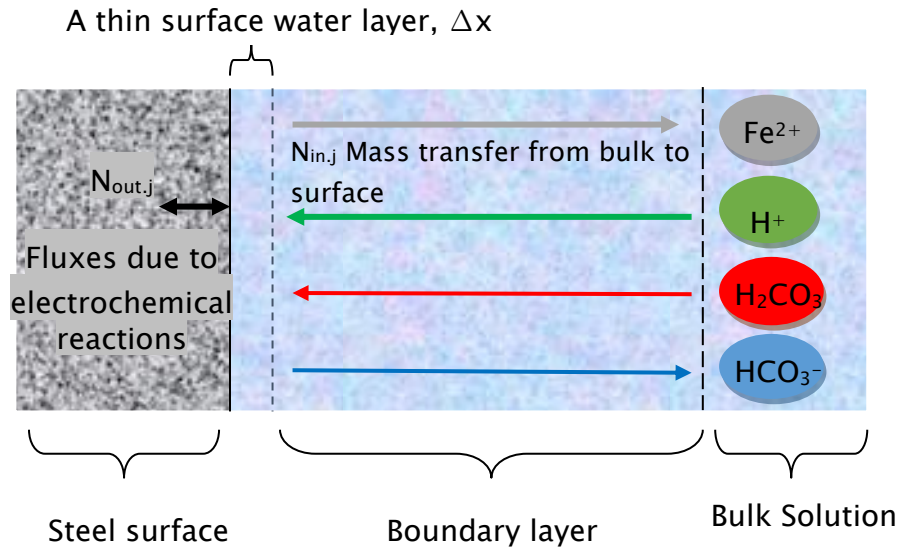
Figure 3 A schematic diagram of two-node model.

Mass Transfer Fluxes

The mass transfer fluxes, $N_{in,j}$ are given by

$$N_{in,j} = k_{m,j}(c_{b,j} - c_{s,j}) \tag{6}$$

where $k_{m,j}$ (m/s) and $c_{b,j}$ (mol/m³) are the mass-transfer coefficient and bulk concentration of species j respectively. Mass-transfer coefficients are generally functions of the geometry and of the Reynolds, Schmidt and Sherwood numbers. Thus, the mass-transfer coefficient for turbulent single phase flow inside a pipe can be calculated using the Berger and Hau [23] correlation:

$$Sh = 0.0165 \times Re^{0.86} \times Sc^{0.33} \tag{7}$$

where the Sherwood number Sh=(kd)/D, in terms of the mass-transfer coefficient, k (m/s), RCE diameter, d (m), and diffusion coefficient D (m²/s), the Reynolds number Re=(U_{RCE} d)/ν, where ν is the kinematic viscosity (m²/s) and the Schmidt number Sc= ν/D.

For an RCE the following Eisenberg correlation [24] has been shown to be accurate for smooth surfaces

10

$$Sh = 0.0791 \, Re^{0.7} Sc^{0.356} \qquad (8)$$

However, for rough surfaces the recent experimental study of Al-Khateeb et al. [2] has shown that the total surface area of the rough surface must be accounted for. They proposed the following correlation for mass transfer for rough samples:

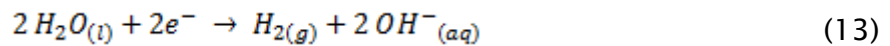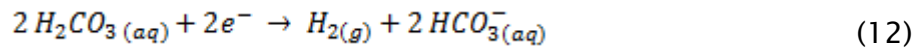$$Sh_R = \frac{f}{2} \, Re \, Sc^{\,0.356} \qquad (9)$$

where Sh_R is the Sherwood number corrected with the total surface area and

$$\frac{f}{2} = 0.0457 \, Re^{-0.2} \qquad (10)$$

The properties of the species depend on temperature and viscosity, and are provided in Tables A.1, with reference diffusion coefficients provided in Table A.2.

5.   Electrochemical Fluxes

The rate of the electrochemical reactions at the metal surface depends on the surface concentrations of species involved in electrochemical reactions and on the temperature [5]. The cathodic reactions are given by the reduction of hydrogen, carbonic acid (via a buffering effect) and water given respectively by

$$2\,H^+_{(aq)} + 2e^- \rightarrow H_{2\,(g)} \qquad (11)$$

$$2\,H_2CO_{3\,(aq)} + 2e^- \rightarrow H_{2(g)} + 2\,HCO^-_{3(aq)} \qquad (12)$$

$$2\,H_2O_{(l)} + 2e^- \rightarrow H_{2(g)} + 2\,OH^-_{(aq)} \qquad (13)$$

It is important to stress that carbonic acid has been shown to contribute to the cathodic reaction via a buffering effect whereby it is transported to the steel surface and dissociates [22], resulting in the reaction shown in equation (12), hence there is a distinction in the pathway, but the ultimate hydrogen evolution reaction is the same.

The anodic reaction is given by equation (14), although this is a simplification and is actually believed to occur through a number of complex, intermediate reactions as described by Nesic et al [25].

11

$$Fe_{(s)} \rightarrow Fe^{2+}{}_{(aq)} + 2\,e^- \tag{14}$$

Since the electrochemical reactions involve exchange of electrons, the reaction rate represents the rate at which electrons are released or consumed. These exchange current densities can be calculated using the following formula:

$$i = \pm i_0 \times 10^{\pm\left(\frac{E\ -E_{rev}}{b}\right)} \tag{15}$$

where i_o is the exchange current density (A/m²), E is the potential of the corroding surface (V), E_{rev} is the reversible potential of a specific reaction (V) and b is the Tafel slope (V). A positive sign refers to the anodic reaction and a negative sign refers to a cathodic one. The exchange current densities take the general form

$$i_o = i_{ref} \left(\frac{c_{H+}}{c_{H+,ref}}\right)^{a1} \left(\frac{c_{co2}}{c_{co2,ref}}\right)^{a2} \left(\frac{c_{H2CO3}}{c_{H2CO3,ref}}\right)^{a3} \; e^{\frac{-\Delta H}{R}\left(\frac{1}{T}-\frac{i}{T_{ref}}\right)} \tag{16}$$

where the reference parameter values and exponents a_1, a_2 and a_3 for each of the reactions are given in Table A.3 in the Appendix.

For the hydrogen reduction reaction the total current density i_{H^+} is given by the harmonic mean of the charge transfer–controlled exchange current, i_{0,H^+}, and the mass–transfer limited current $i_{lim,H+} = F\,K_{m,H+}\,C_{b,H+}$, [26], namely

$$\frac{1}{i_{H+}} = \frac{1}{i_{a\,H+}} + \frac{1}{i_{lim\,H+}} \tag{17}$$

The total current density for carbonic acid is calculated similarly, with

$$\frac{1}{i_{H2CO3}} = \frac{1}{i_{a\,H2CO3}} + \frac{1}{i_{lim\,H2CO3}} \tag{18}$$

where

$$i_{lim\,H2CO3} = f_o\; F\; C_{b,co2}\,\sqrt{D_{H2CO3}\,K_{hy}\,k_{f,hy}} \tag{19}$$

F=96485 C/mol is Faraday's constant and f_o is the flow factor for the limiting current of carbonic acid. The latter is defined by:

$$f_o = coth\ (\zeta) \tag{19}$$

ζ is the ratio of thickness of mass transfer diffusion layer to reaction layer (δ_m/δ_r)

$$\delta_m = \frac{D_{H2CO3}}{K_{m,H2CO3}} \tag{20}$$

$$\delta_r = \sqrt{\frac{D_{H2CO3}}{K_{b,hy}}} \tag{21}$$

For spontaneous corrosion the potential, E, at the corroding surface can be found by equating the total cathodic and anodic current densities:

$$\sum_{I}^{n_a} i_a = \sum_{I}^{n_c} i_c \tag{22}$$

Once E is determined, the electrochemical fluxes of species can be calculated from equations (15) and (16) to yield

$$N_{out,i} = \pm \frac{i_i}{n_i\ F} \tag{23}$$

where n_i is the number of moles of electrons created per mole of species in the ith electrochemical reaction: $n_i=1$ for all cathodic reactions and 2 for the anodic reaction. A positive or negative sign is taken for cathodic and anodic reactions, respectively.

6.   Chemical Reactions

For CO_2 corrosion, the water chemistry is determined by the combined effects of CO_2 dissolution, carbonic acid hydration, carbonic acid dissociation, bicarbonate ion dissociation and water dissociation. These reactions are respectively

$$CO_{2\,(g)} \Longleftrightarrow CO_{2\,(aq)} \tag{24}$$

$$CO_{2(aq)} + H_2O \Leftrightarrow H_2CO_3 \tag{25}$$

$$H_2CO_3 \Leftrightarrow H^+ + HCO_3^- \tag{26}$$

$$HCO_3^- \Leftrightarrow H^+ + CO_3^{2-} \tag{27}$$

$$H_2O \Leftrightarrow H^+ + OH^- \tag{28}$$

The rates of each of these reactions depend on temperature, CO_2 partial pressure and ionic strength [5]. The reaction rate constants used here are given in Table A.4 in the Appendix.

In the bulk, the equations for the 6 different species (CO_2, H_2CO_3, HCO_3^-, CO_3^{2-}, OH^- and H^+) are created as follows. Firstly, CO_2 molecules are created by carbonic acid hydration:

$$R_{CO_2} = \frac{d}{dt}\left(c_{CO_2}\right) = K_{b,hy}\, c_{H_2CO_3} - K_{f,hy} c_{CO_2} \tag{29}$$

H_2CO_3 is created by carbonic acid hydration and carbonic acid dissociation:

$$R_{H_2CO_3} = \frac{d}{dt}\left(c_{H_2CO_3}\right) = -\left(K_{b,hy}\, c_{H_2CO_3} - K_{f,hy} c_{CO_2}\right) - \left(K_{f,ca}\, c_{H_2CO_3} - K_{b,ca} c_{H^+} c_{HCO_3^-}\right) \tag{30}$$

HCO_3^- ions are created by carbonic acid dissociation and bicarbonate ion dissociation:

$$R_{HCO_3^-} = \frac{dc_{HCO_3^-}}{dt} = \left(K_{f,ca}\, c_{H_2CO_3} - K_{b,ca} c_{H^+} c_{HCO_3^-}\right) - \left(K_{f,bi}\, c_{HCO_3^-} - K_{b,bi} c_{H^+} c_{CO_3^{2-}}\right) \tag{31}$$

CO_3^{2-} ions are created by bicarbonate ion dissociation:

$$R_{CO_3^{2-}} = \frac{dc_{CO_3^{2-}}}{dt} = \left(K_{f,bi}\, c_{HCO_3^-} - K_{b,bi} c_{H^+} c_{CO_3^{2-}}\right) \tag{32}$$

OH^- ions are created from water dissociation:

$$R_{OH^-} = \frac{dc_{OH^-}}{dt} = K_{f,wa} - K_{b,wa} c_{H^+} c_{OH^-} \tag{33}$$

H^+ ions are created by carbonic acid dissociation, bicarbonate ion dissociation and water dissociation:

$$R_{H^+} = \frac{dc_{H^+}}{dt} = \left(K_{f,ca}\, c_{H_2CO_3} - K_{b,ca}c_{H^+}c_{HCO_3^-,}\right) + \left(K_{f,bi}\, c_{HCO_3^-,} - K_{b,bi}c_{H^+}c_{CO_3^{2-},}\right) + (K_{f,wa}$$
$$- K_{b,wa}c_{H^+}c_{OH^-})$$

(34)

Equations (29–34) for the 6 different species (CO_2, H_2CO_3, HCO_3^-, CO_3^{2-}, OH^- and H^+) in the bulk are solved using an efficient Newton–Raphson numerical scheme implemented in Python.

7. Steady–state Corrosion Model

This study investigates the effect of surface roughness of corrosion rates in non–film-forming conditions where corrosion rate attains a steady–state. In this case it can be shown, [27], that the 2-node model can be re-cast into the following simplified form:

$$0 = -\frac{\left(i_{H^+} + i_{H_2O} + i_{H_2CO_3}\right)}{F} + k_{m,H^+}\left(c_{H_b^+} - c_{H_s^+}\right) - k_{m,OH^-}\left(c_{OH_b^-} - c_{OH_s^-}\right) + k_{m,CO_2}\left(c_{CO_{2,b}} - c_{CO_{2,s}}\right) -$$
$$k_{m,CO_3^{2-}}\left(c_{CO_{3,b}^{2-}} - c_{CO_{3,s}^{2-}}\right) + k_{m,H_2CO_3}\left(c_{H_2CO_{3,b}} - c_{H_2CO_{3,s}}\right)$$

(35)

$$10^6 K_{wa} = c_{H_s^+}c_{OH_s^-}$$

(36)

$$0 = k_{m,CO_2}\left(c_{CO_{2,b}} - c_{CO_{2,s}}\right) + \Delta x(K_{b,hy}\, c_{H_2CO_{3,s}} - K_{f,hy}c_{CO_{2,s}})$$

(37)

$$0 = k_{m,CO_2}\left(c_{CO_{2,b}} - c_{CO_{2,s}}\right) + k_{m,H_2CO_3}\left(c_{H_2CO_{3,b}} - c_{H_2CO_{3,s}}\right) + + k_{m,HCO_3^-}\left(c_{HCO_{3,b}^-} - c_{HCO_{3,s}^-}\right) +$$
$$k_{m,CO_3^{2-}}\left(c_{CO_{3,b}^{2-}} - c_{CO_{3,s}^{2-}}\right)$$

(38)

$$c_{H_s^+}c_{HCO_{3,s}^-} = 1000\, K_{Ca}\, c_{H_2CO_{3,s}}$$

(39)

$$c_{H_s^+}c_{CO_{3,s}^{2-}} = 1000\, K_{bi}c_{HCO_{3,s}^-}$$

(40)

$$\frac{\partial c_{Fe_s^{2+}}}{\partial t} = 0 = \frac{i_{Fe^{2+}}}{2F} + k_{m,Fe^{2+}}\left(c_{Fe_b^{2+}} - c_{Fe_s^{2+}}\right)$$

(41)

These 7 equations are solved using a Newton–Raphson numerical scheme implemented in Python. Once $i_{Fe^{2+}}$ (A/m²) has been determined the corrosion rate in mm/year is $1.16 \times i_{Fe^{2+}}$.

15

8. Experimental and Theoretical Results

Model Validation

The chemical solver is validated first. Solutions of equation (29)-(34) for the bulk chemistry are validated against the experimental results of Meyssami et al. [28] and Tanupabrungsun et al. [29]. These are shown in Figure 4. Agreement is excellent in both cases.
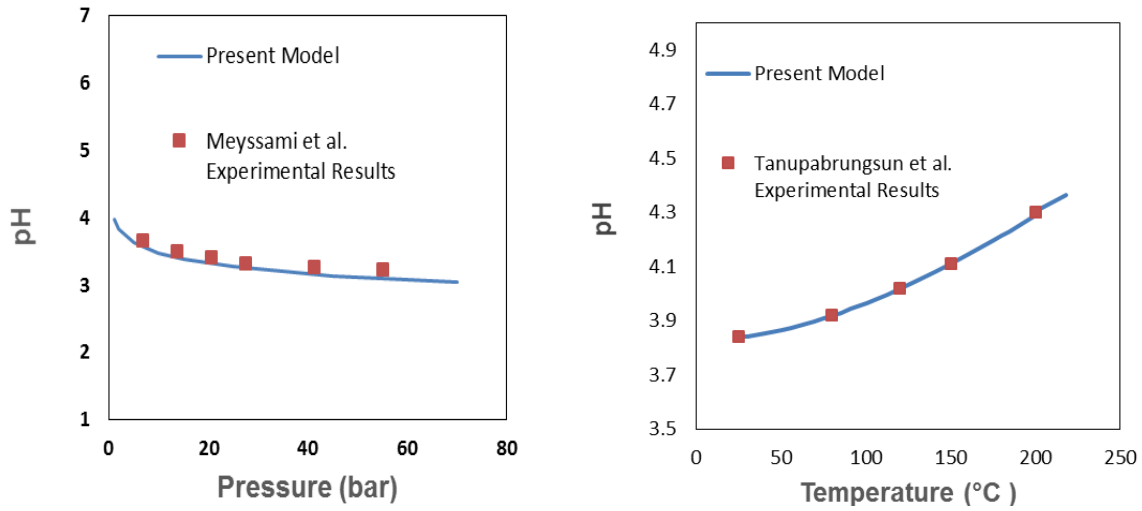

Figure 4 Validation of bulk chemistry predictions against Meyssami et al. [28] and Tanupabrungsun et al. [29].

The corrosion rate predictions obtained here are now compared with the pipe flow loop experiments for smooth surfaces and corrosion model predictions for different pH values and flow speeds from Zheng et al. [1] in Figure 5, using the Berger & Hau correlation for mass-transfer coefficient.
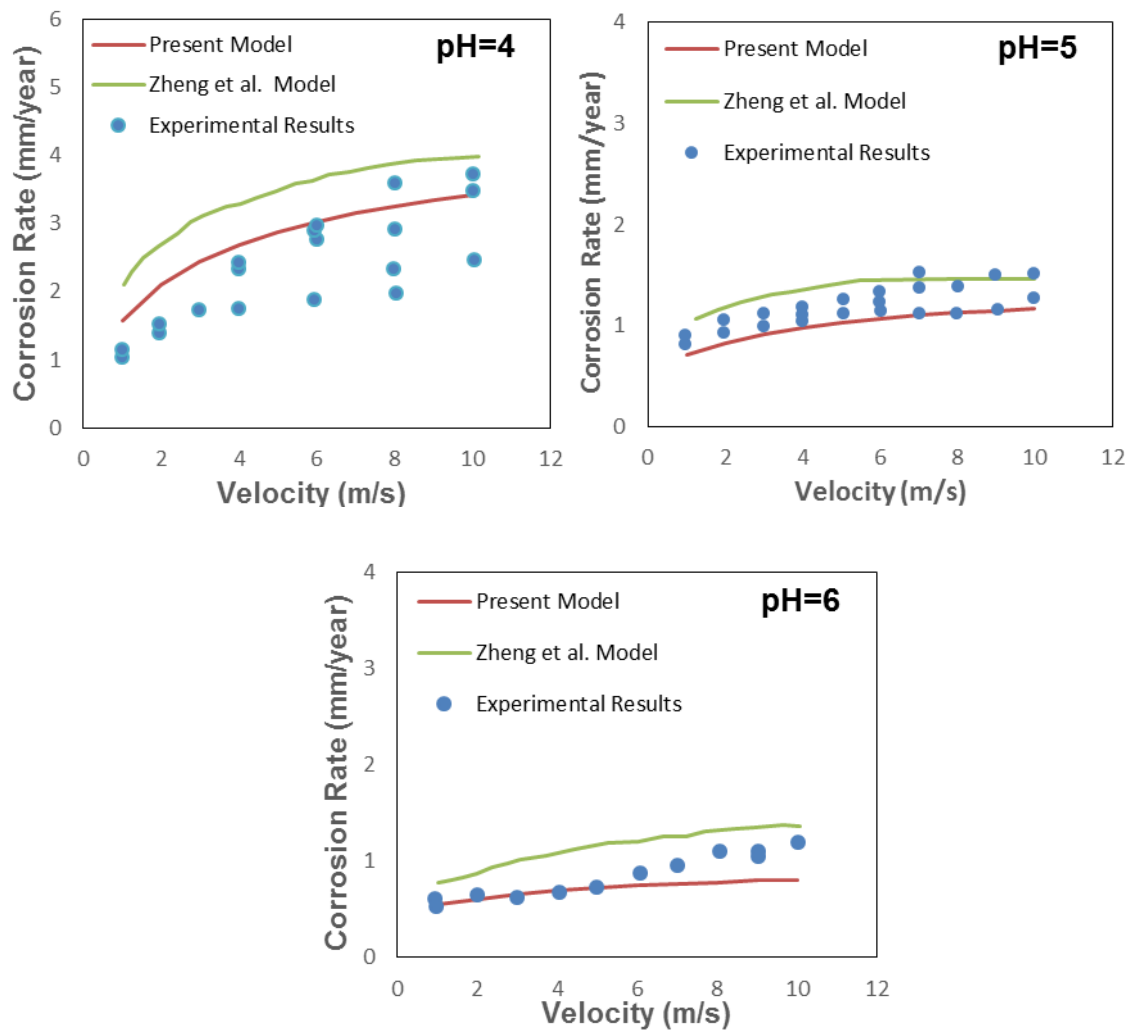
Figure 5 Comparisons between the present model predictions for pipe flow against experiments and predictions of Zheng et al. [1] at 1 bar CO_2, 20°C, d=0.01m, for a range of pH values and velocities.

The present corrosion model predictions agree reasonably well with both the experimental and theoretical results of Zheng et al. [1]. The prediction that corrosion rates are independent of flow speed for pH=6 indicates that the process is predominantly activation-controlled rather than mass-transfer controlled in these cases.

A new series of experimental measurements and theoretical predictions of corrosion rate for RCE systems in aqueous CO_2 solutions, with both smooth and

rough surfaces, is now presented. For smooth RCE samples, corrosion rate values from the RCE experiments were compared with the model's predictions by varying the solution pH and the rotational speed of the RCE. The effect of velocity was studied at pH=4, 5 and 6. The rotation speed started with 1000 rpm (0.628 m/s) and increased up to 4000 rpm (2.512 m/s).
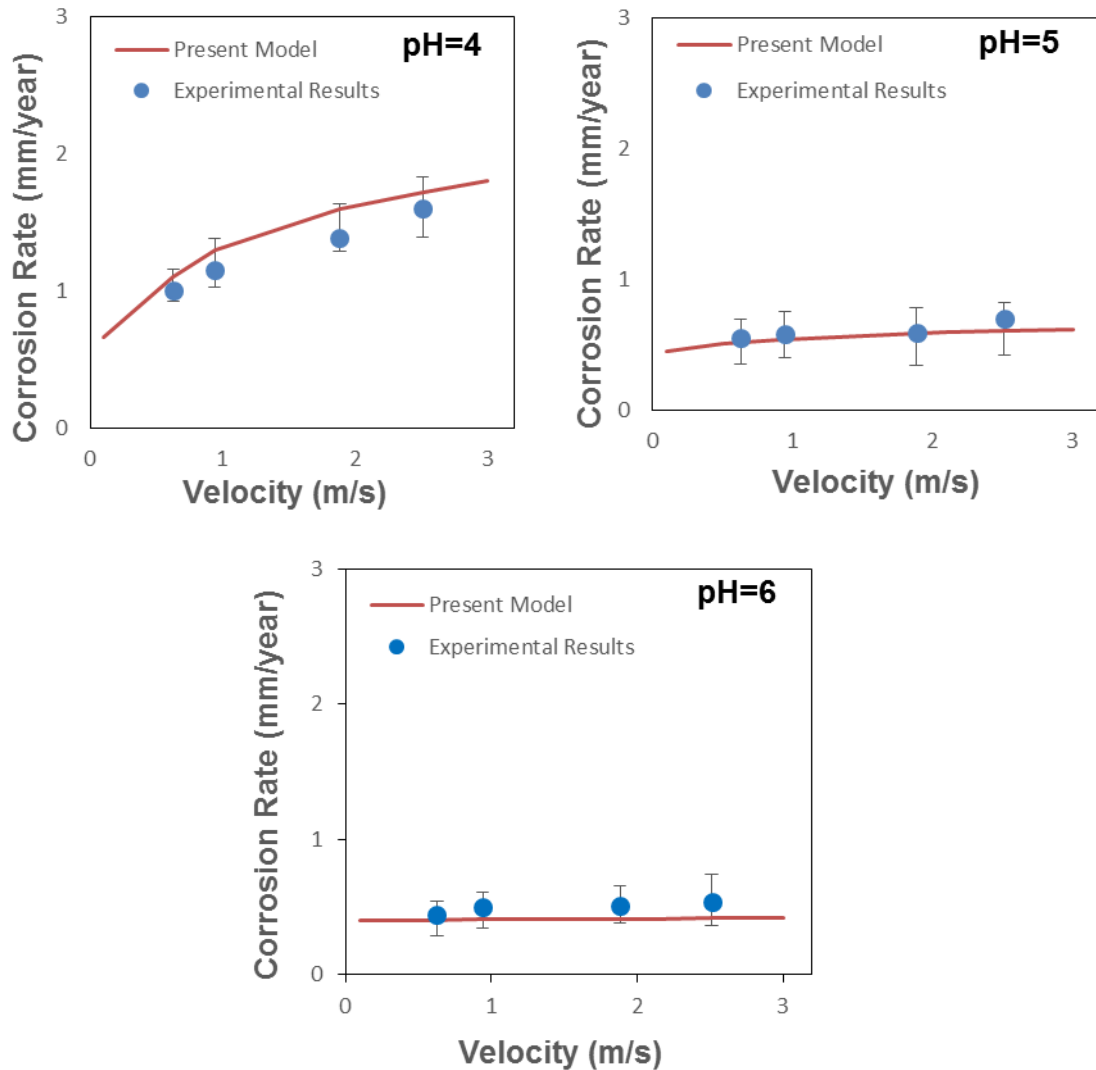

Figure 6 Comparisons between experimental and theoretical corrosion rates at 1 bar total pressure, 25℃, various pH, and different rotation speeds for a smooth RCE.

Figure 6 shows that for pH=4 corrosion rate increases with rotational speed, indicating that mass-transfer from the bulk is important, whereas for the higher pH values, where the bulk concentration of H^+ are orders of magnitude smaller, mass transfer of H^+ ions is far less important. This leads to a reduction in the cathodic consumption of H^+ ions and a corresponding reduction in corrosion rate. Good agreement was obtained between the model predictions and the experimental results for all cases considered. The average difference between the model and the experiments is about 14, 10 and 18 % for pH=4, 5 and 6 respectively.

It is generally accepted that an increase in surface roughness leads to higher corrosion rates, since rough surfaces have a larger interfacial area with the corrosive environment and can induced localised mass transfer between surface peaks [30]. However, few studies have quantified the effect of the increase in surface area on the values of corrosion rates in CO_2 environments. The work of Asma et al. [31] studied the effect of surface finish on corrosion rates at room temperature. Their results revealed that the increase in degree of roughness leads to increase in corrosion rate. This was attributed to the larger surface which is in contact with corrosion environment. However, they did not correct for the actual surface area nor was the effect of surface roughness on mass-transfer quantified as experiments were performed in static conditions.

The first series of experiments on rough surfaces in this work were also carried out in static conditions and normalised based on their actual surface area determined by profilometry, as opposed to their projected area. The purpose of this analysis was to confirm that the machining of the test samples did not modify or cold work the surface such that the corrosion rate of the material was enhanced. Tests were performed with four samples of different surface finishes of X65 carbon steel in a 1 wt.% NaCl solution saturated with CO_2. The pH and temperature were 4 and 25℃ respectively. Figure 7 presents the corrosion rate results after correcting with the real surface area. It is clear that correcting for area leads to no significant change in corrosion rates across all rough surfaces, indicating that the machining process does not influence the dissolution behaviour of the steel.
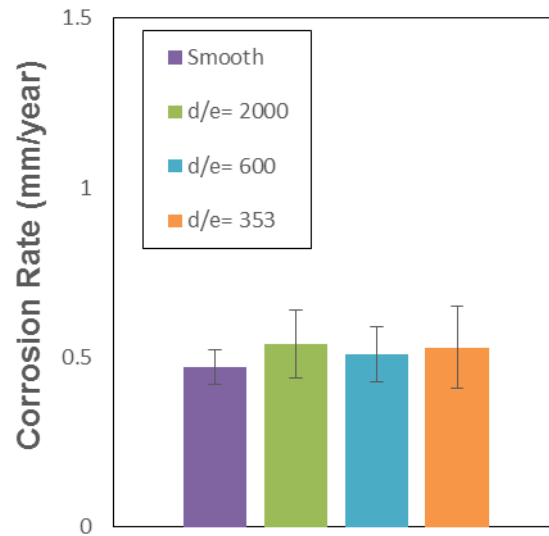
Figure 7 Static corrosion rate experimental results at 1 bar total pressure in a CO_2-saturated 1 wt% NaCl solution at pH=4, 25℃, for different surface finishes after correcting for total surface area. Note: area ratios are shown in Table 1.

These tests were then extended to cases of turbulent flow over rough carbon steel X65 surfaces. The mass-transfer coefficients used in the 2-node corrosion model are calculated using the new correlation for mass-transfer to rough RCE surfaces proposed by Al-Khateeb et al. [2], (equations (9) and (10)). All current densities, and hence the corrosion rate, were scaled with respect to the total surface area measured using white light interferometry. Figure 8 shows the experimental and theoretical corrosion rate results as a function of RCE velocity for each of the four different roughness values. It is very clear that the corrosion rate increases with the surface roughness. For example, at 3000 rpm the corrosion rate increases by roughly 12, 22 and 31 %, compared to the smooth sample, as the surface roughness increases. The modified 2-node model also agrees very well for all roughness cases with average discrepancies of 10, 12, 5 and 6.5 % in comparison with the experiments for the four roughness cases. The average difference between the model and the experiments is around 8.5% and the maximum deviation is 17%.
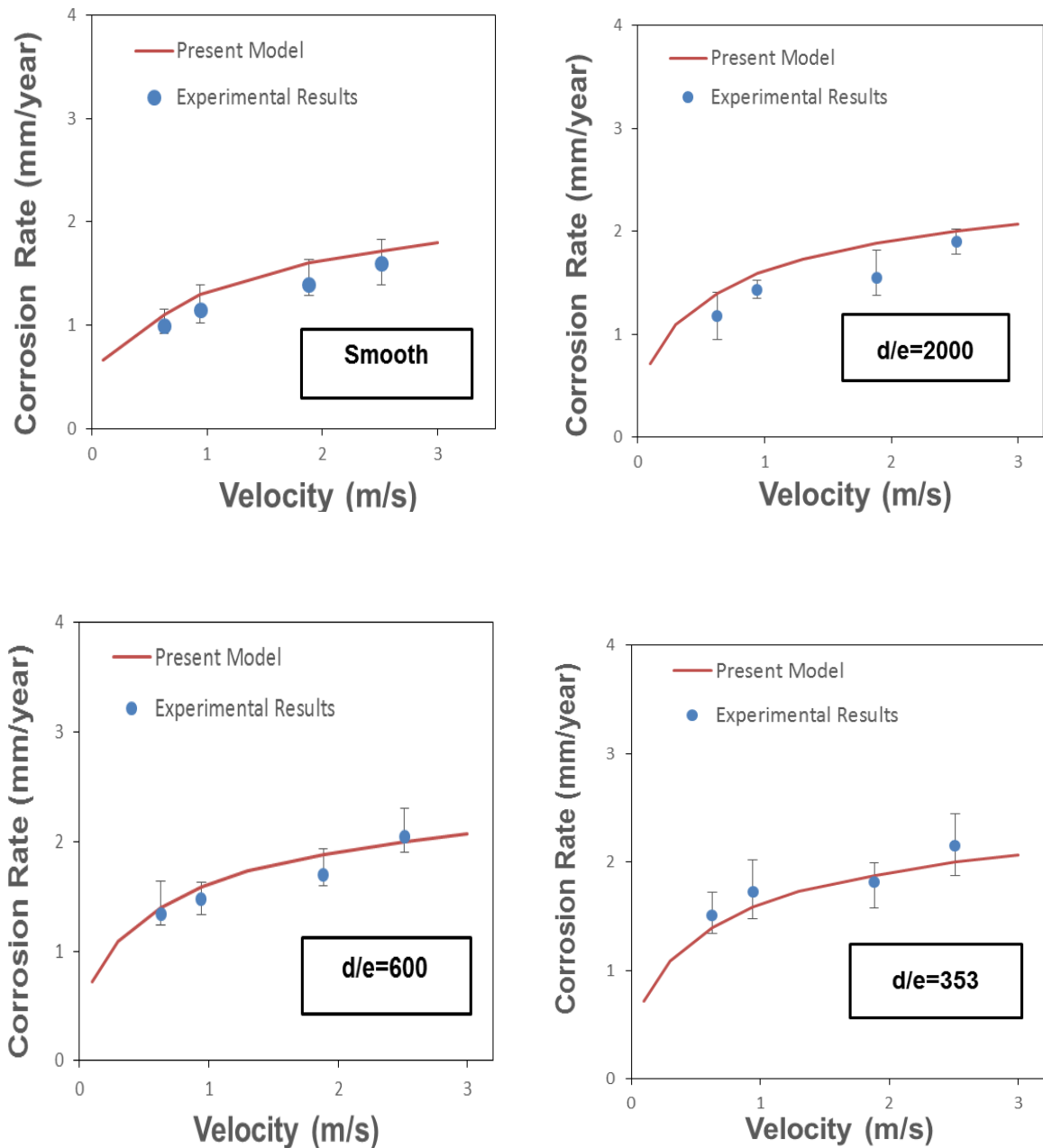
Figure 8 Comparisons between model results and experiment results at 1 bar total pressure, 25°C, various pH, and different rotation speed for different surface finishes.

Several explanations for the effect of surface roughness on increasing corrosion rate has been discussed in the literature. It is generally assumed that the roughness peaks disturb the viscous layer and the turbulence generated reduces the resistance to mass transfer across the concentration boundary layer and in the valleys between

the roughness peaks [32]. The analysis of mass-transfer intensification is based on behaviour of turbulent eddies. These eddies penetrate into a cavity on a wall causing deceleration in their motion due to viscous friction with the surface. The process of deceleration is non uniform and causes the formation of areas where turbulence fluctuations have relatively high kinetic energies at distances from the surface which are significantly smaller than the diffusive layer thickness. These fluctuations in turn cause localised regions of high mass-transfer [33].

Conclusion

The RCE experiments have shown that surface roughness is very influential and leads to a monotonic increase in corrosion rate as surface roughness increases. Results presented here have shown that it is very important to measure the total surface area of rough surfaces since this is the appropriate area for calculating corrosion current densities for comparison with the numerous mass-transfer correlations in the literature.

Reliable corrosion rate prediction models can be very useful for designing pipeline networks and critical infrastructure in oil and gas production and nuclear processing industries. Since pipelines will inevitably have non-negligible surface roughness which increase corrosion rates compared to smooth scenarios, it is important to develop understanding and accurate prediction models which can account for surface roughness. The RCE experiments carried out here have shown that coupling the well-known Eisenberg mass-transfer correlation into the 2-node corrosion model proposed recently by Zheng et al. [1] can predict corrosion rates accurately for smooth surfaces. For rough surfaces, the Eisenberg correlation is inadequate, and should be replaced by a correlation which accounts for surface roughness and total surface area. This study has shown that a new correlation for mass transfer coefficient, equations (9) and (10), can be used within the 2-node modelling approach to predict corrosion rate from rough surfaces accurately. In the present study the discrepancy between experimental and predicted corrosion rates is typically around 8.5%.

Despite the success of the 2-node model, there is a need for far greater understanding of the physical mechanisms by which roughness accelerates the corrosion rate. Recent advances in high fidelity Computational Fluid Dynamics, Busse et al. [34] are developing the ability to resolve the important localised flow

features over rough surfaces, and will further aid both the physical understanding and predictive capability of complex mass transfer processes over rough surfaces.

Appendix

Table A.1 Species properties as a function of Temperature [35].

Density	$\rho(T) = 1152.3 - 0.5116T$
Dynamic viscosity	$\mu(T) = \mu_{ref} \times 10^{\frac{1.3272(20-T)-0.001053(20-T)^2}{T+105}}$
Diffusion coefficient	$D = D_{ref}\left(\dfrac{T}{T_{ref}}\right)\left(\dfrac{\mu_{ref}}{\mu}\right)$
T_{ref} is the reference temperature $=20°C$, $\mu_{ref}=1.002$ kg/(m.s)	

Table A.2: Reference Diffusion Coefficients for Each Species in the Model

Species	Diffusion Coefficients (m²/s)	Reference
CO_2	1.96×10^{-9}	[36]
H_2CO_3	2×10^{-9}	[37]
HCO_3^-	1.105×10^{-9}	[5]
CO_3^{2-}	0.92×10^{-9}	[37]
H^+	9.312×10^{-9}	[5]
OH^-	5.26×10^{-9}	[5]
Fe^{2+}	0.72×10^{-9}	[37]

The exchange current density is $i_o = i_{ref} \left(\dfrac{c_{H+}}{c_{H+,ref}}\right)^{a1} \left(\dfrac{c_{co2}}{c_{co2,ref}}\right)^{a2} \left(\dfrac{c_{H2CO3}}{c_{H2CO3,ref}}\right)^{a3} e^{\frac{-\Delta H}{R}\left(\frac{1}{T}-\frac{i}{T_{ref}}\right)}$

	i_{ref}	a_1	$c_{H+,ref}$	a_2	$c_{co2,ref}$	a_3	$c_{H2CO3,ref}$	ΔH	T_{ref}	E_{rev}	b
	A/m²		molar		molar		molar	KJ/mol	°C	V	V
$2H^+ +2e \rightarrow H_2$	0.05	0.5	10^{-4}	0	N/A	0	N/A	30	25	$\dfrac{-2.303RT}{F}pH$	$\dfrac{2.303\ RT}{0.5\ F}$
$2H_2CO_3 +2e \rightarrow HCO_3 +H_2$	0.018	- 0.5	10^{-5}	0	N/A	1	10^{-4}	50	20	$\dfrac{-2.303RT}{F}pH$	$\dfrac{2.303\ RT}{0.5\ F}$
$2H_2O +2e \rightarrow H_2 + 2OH^-$	0.002	0	N/A	0	N/A	0	N/A	30	25	$\dfrac{-2.303RT}{F}pH$	$\dfrac{2.303\ RT}{0.5\ F}$
$Fe \rightarrow Fe^{2+} +2e$	0.1 (RCE) 1 (pipe)	2 for pH<4 1 for 4<pH<5 0 for pH>5	10^{-4}	1 for P_{CO2} <1bar 0 for P_{CO2} >1bar	0.0366	0	N/A	37.5	25	-0.488	$\dfrac{2.303\ RT}{1.5\ F}$

Table A.4 Chemical reaction rate constants

The chemical constants used here are given below, together with their source references. Note: T_f is the temperature in degree Fahrenheit, T absolute temperature in Kelvin, T_c is the temperature in Celsius, I is the ionic strength in molar, and p is the total pressure in psi.

$$K_{sol} \frac{14.5}{1.00258} \times 10^{-(2.27+5.65\times10^{-3}\times T_f - 8.06\times10^{-6}\times T_f^2 + 0.075\times I)} \text{ (molar/bar) [39]}$$

$$K_{wa} = 10^{-(29.3868 - 0.0737549\times T_k + 7.47881\times 10^{-5}\times T_k^2)} \text{ (molar}^2) \text{ [40]}$$

$$K_{b\,wa} = 7.85 \times 10^{10} \text{ (molar}^{-1} \text{ s}^{-1}) \text{ [41]}$$

$$K_{hy} = 2.58 \times 10^{-3} \text{ [42]}$$

$$K_{f\,hy} = 10^{329.85 - 110.541\times\log T_k - \frac{17265.4}{T_k}} \text{ (s}^{-1}) \text{ [42]}$$

$$K_{ca} = 387.6 \times 10^{-(6.41 - 1.594\times 10^{-3} T_f + 8.52*10^{-6} T_f^2 - 3.07\times10^{-5} P - 0.4772\times I^{0.5} + 0.118\times I)} \text{ [39]}$$

$$K_{f\,ca} = 10^{5.71 + 0.0526\times T_c - 2.94\times 10^{-4} T_c^2 + 7.91\times10^{-7}\times T_c^3} \text{ (s}^{-1}) \text{ [5]}$$

$$K_{bi} = 10^{-(10.61 - 4.97\times 10^{-3} T_f + 1.331*10^{-5}\times T_f^2 - 2.624\times 10^{-5} P - 1.166\times I^{0.5} + 0.3466\times I)} \text{ (molar) [39]}$$

$$K_{f\,bi} = 10^9 \text{ (s}^{-1}) \text{ [5]}$$

$$K = k_f / k_b$$

References

1.	Zheng, Y. Ning, J., Brown, B., Nesic, S. *Advancement in predictive modeling of mild steel in CO_2- and H_2S-containign environments. Corrosion*, **72**(5), 679-691, 2016.

2.	Al-Khateeb, Barker, R. Neville, A. Thompson, H.M. *The role of surface roughness on mass transfer in CO2-containing oil and gas environments*. Submitted to Corrosion Journal (under review), 2017.

3.	Kermani, M.B. and Morshed, A., *Carbon Dioxide Corrosion in Oil and Gas ProductionA Compendium, Corrosion* 59.8 (2003): 659-683*.*

4.	Fogg, G. and Morse, J. *Development of a new solvent-free flow efficiency coating for natural gas pipelines*. in *Rio Pipeline 2005 Conference and Exposition, IBP1233*. 2005.

5.	Nordsveen, M., Nesic, N., Nyborg, R., Stangeland, A. *A mechanistic model for carbon dioxide corrosion of mild steel in the presence of protective iron carbonate films-Part 1*: Theory and verification. Corrosion, **59**(5): p. 443-456, 2003.

6.	Poulson, B., *Mass transfer from rough surfaces.* Corrosion Science, 1990. **30**(6): p. 743-746.

7.	Tantirige, S. and Trass, O., *Mass transfer at geometrically dissimilar rough surfaces.* The Canadian Journal of Chemical Engineering, 1984. **62**(4): p. 490-496.

8.	Postlethwaite, J. and Lotz, U., *Mass transfer at erosion-corrosion roughened surfaces.* The Canadian Journal of Chemical Engineering, 1988. **66**(1): p. 75-78.

9.	Cornet, I., Lewis, W., and Kappesser, R., *Effect of surface roughness on mass transfer to a rotating disc.* Trans inst Chem eng, 1969. **47**(7): p. 222-226.

10.	Gabe, D. and Makanjuola, P., *Enhanced mass transfer using roughened rotating cylinder electrodes in turbulent flow.* Journal of Applied Electrochemistry, 1987. **17**(2): p. 370-384.

11.	King, C.V. and Howard, P.L., *Heat Transfer and Diffusion Rates at Solid-Liquid Boundaries.* Industrial & Engineering Chemistry, 1937. **29**(1): p. 75-78.

12.	Ibl, N., *Advances in electrochemistry and electrochemical engineering: edited by P. Delahay and CW Tobias, vol. 1 (edited by P. Delahay) 326 pages, $12, Interscience, New York 1961*. 1962, Pergamon.

13.	Brenan, W.C. and Trass, O., *52nd Nat. Meeting of A. I. Ch. E. (1964).*

14. Walsh, F. C., Kear, G., Nahle, A. H., Wharton, J. A., & Arenas, L. F. *The rotating cylinder electrode for studies of corrosion engineering and protection of metals—An illustrated review. Corrosion Science.,*2017.

15. Kahyarian, A., Singer, M., and Nesic, S., *Modeling of uniform CO_2 corrosion of mild steel in gas transportation systems: A review.* Journal of Natural Gas Science and Engineering, 2016. **29**: p. 530-549.

16. De Waard, C. and Milliams, D., *Carbonic acid corrosion of steel.* Corrosion, 1975. **31**(5): p. 177-181.

17. Pots, B.F.M., John, R.C., Rippon, I.J., Thomas, M.J.J.S., Kapusta, S.D., Grigs, M.M., Whitham, T. *Improvements on the deWaard-Milliams Corrosion Prediction and Applications to Corrosion Management.* NACE International, Paper 235, 2002.

18. Olson, S. *Corrosion prediction by use of the Norsok M-506 model – guidelines and limitations.* NACE International. Paper no. 263, 2003.

19. Nešić, S., *Key issues related to modelling of internal corrosion of oil and gas pipelines – A review.* Corrosion Science, 2007. **49**(12): p. 4308-4338.

20. Sudaram, M., Raman, V., High, M.S., tree, D. Wagner, J. *Determinisitic modelling of corrosion in downhole environments.* NACE International. Paper No. 30. 1996

21. Han, J., Carey, J.W., and Zhang, J., *A coupled electrochemical–geochemical model of corrosion for mild steel in high-pressure CO 2–saline environments.* International Journal of Greenhouse Gas Control, 2011. **5**(4): p. 777-787.

22. Remita, E., Tribollet, B., Sutter, E., Vivier, V., Ropital, F., Kittel, J. *Hydrogen evolution in aqueous solutions containing dissolved CO2: quantitative contribution of the buffering effect.* Corrosion Science, 2008. **50**(5): p. 1433-1440.

23. Berger, F. and Hau, K.-F.-L., *Mass transfer in turbulent pipe flow measured by the electrochemical method.* International Journal of Heat and Mass Transfer, 1977. **20**(11): p. 1185-1194.

24. Eisenberg, M., Tobias, C., and Wilke, C., *Ionic mass transfer and concentration polarization at rotating electrodes.* Journal of the Electrochemical Society, 1954. **101**(6): p. 306-320.

25. Nesic, S., Thevenot, N., Crolet, J. L., & Drazic, D. M.,*Electrochemical properties of iron dissolution in the presence of CO_2 Basics revisited.* No. CONF-960389--. NACE International, Houston, TX (United States), 1996.

26. Zheng, Y., Ning, J., Brown, B., & Nešić, S*., Electrochemical Model of Mild Steel Corrosion in a Mixed H_2S/CO_2 Aqueous Environment.* CORROSION/2014, paper, 2014(3907).

27.   Zheng, Y. Electrochemical mechanism and model of H_2S corrosion of carbon steel, PhD thesis, Ohio University, 2015.

28.   Meyssami, B., Balaban, M.O., and Teixeira, A.A., *Prediction of pH in model systems pressurized with carbon dioxide.* Biotechnology progress, 1992. **8**(2): p. 149-154.

29.   Tanupabrungsun, T., Young, D., Brown, B., & Nešic, S*., Construction and verification of pourbaix diagrams for CO2 corrosion of mild steel valid up to 250 C.* in *CORROSION 2012.* 2012. NACE International.

30.   Evgeny, B., Hughes, T., and Eskin, D., *Effect of surface roughness on corrosion behaviour of low carbon steel in inhibited 4 M hydrochloric acid under laminar and turbulent flow conditions.* Corrosion Science, 2016. **103**: p. 196-205.

31.   Asma, R., Yuli, P., and Mokhtar, C., *Study on the effect of surface finish on corrosion of carbon steel in CO2 environment.* Journal of Applied Sciences, 2011. **11**(11): p. 2053-2057.

32.   Dawson, D.A. and Trass, O., *Mass transfer at rough surfaces.* International Journal of Heat and Mass Transfer, 1972. **15**(7): p. 1317-1336.

33.   Levich, V.G., *Physicochemical hydrodynamics.* 1962: Prentice hall.

34.   Busse, A., Lützner, M., and Sandham, N.D., *Direct numerical simulation of turbulent flow over a rough surface based on a surface scan.* Computers & Fluids, 2015. **116**: p. 129-147.

35.   Nesic, S., Postlethwaite, J., and Olsen, S., *An electrochemical model for prediction of corrosion of mild steel in aqueous carbon dioxide solutions.* Corrosion, 1996. **52**(4): p. 280-294.

36.   Perry, R. and Green, D., *Handbook of chemical engineering.* pg, 1984: p. 17-6.

37.   Kvarekvål, J., *A kinetic model for calculating concentration profiles and fluxes of CO_2 related species across the Nernst diffusion layer.* 1997, NACE International, Houston, TX (United States).

38.   Fardisi, S., Tajallipour, N., and Teevens, P.J., *Predicting General Corrosion Rates In Sour Environments With the Growth of a Protective Iron Sulphide Film.* NACE International.

39.   Oddo, J.E. and Tomson, M.B., *Simplified calculation of $CaCO_3$ saturation at high temperatures and pressures in brine solutions.* Journal of Petroleum Technology, 1982. **34**(07): p. 1,583-1,590.

40.   Kharaka, Y.K., et al., *SOLMINEQ., A computer program for geochemical modeling of water-rock interactions.* US geological survey water-resources investigation report, 1988. **88**: p. 4227.

41.   Delahay, P., *Implications of the Kinetics of Ionic Dissociation with Regard to Some Electrochemical Processes—Application to Polarography.* Journal of the American Chemical Society, 1952. **74**(14): p. 3497-3500.

42.   Palmer, D.A. and Van Eldik, R., *The chemistry of metal carbonato and carbon dioxide complexes.* Chemical Reviews, 1983. **83**(6): p. 651-731.